MgO Effect on The Dielectric Properties of $BaTiO_3$

Samira Boumous
Laboratory of Electrical Engineering and Renewable Energy, Mohamed Cherif Messaidia University, Souk Ahras, Algeria
boumous@yahoo.fr

Saad Belkhiat
Laboratory DACHR, Ferhat Abbas Setif University 1, Setif, Algeria
belsa_set@yahoo.fr

Faicel Kharchouche
Laboratory DACHR, Ferhat Abbas Setif University 1, Setif, Algeria
Kharchouche.electro@yahoo.fr

***Abstract*—The dielectric properties of barium titanate as functions of the MgO addition in various rates are investigated in this paper. The ceramics were prepared by conventional methods. X-ray diffraction, scanning electron microscopy and energy dispersive spectrometry, were applied to determine the structure and microstructure of the studied material. Phases MgO, TiO and TiO_2, have been detected. Decrease of the grain size with increasing MgO content was observed. Measurements of εr, tgδ and resistance have been performed at temperatures ranging from 30^0C to 400^0C. The electric permittivity (ε_r) showed a considerable decrease with increasing MgO concentration. Additionally, for low MgO concentration (10≤mol.% MgO) a shift of the dielectric loss peak ($tg\delta_m$) towards low temperatures was observed. When the MgO content was ≥15mol.% MgO the $tg\delta_m$ moved into higher temperatures. The obtained results indicate that the substitution of Mg^{2+} ions in B-site ions (Ti^{4+}) had a significant influence on the values of εr, tgδ and the resistance increase of the ceramics.**

Keywords-$BaTiO_3$; MgO-doped $BaTiO_3$; thermistors PTC; dielectric properties; electric permittivity

I. INTRODUCTION

Barium titanate ($BaTiO_3$) is considered one of the most promising systems for applications in electro-optic devices, memory devices, temperature sensors, time delay circuits, current limiters, current stabilizers and capacitors [1]. $BaTiO_3$ is used as doping in other electrical engineering applications such as varistors [2] and in polymer composites like cable insulation sheaths [3, 4]. The dielectric and ferroelectric properties of $BaTiO_3$ can be efficiently controlled by dopant addition. $BaTiO_3$ is used in electric devices manufactured to work at temperatures less than its Curie temperature (T_c=120°C). In devices functioning at a temperature other than 120°C, it is mixed with other materials such as Mg, $PbTiO_3$ (PT), Zr oxide, and other oxides, in order to shift T_c, above or under 120°C [5-11]. Pure $BaTiO_3$ exhibits very high electric permittivity, since it has positive -temperature-coefficient resistivity (PTCR) above the Curie temperature [12, 13]. This phenomenon was considered as a consequence of the double Schottky barrier, formed at the grain boundaries and of the strong temperature dependence [14]. The PTCR phenomenon of doped $BaTiO_3$, has been explained in [13, 15]. It has been concluded that the PTCR effect is caused by defect distribution in the samples. The effects of sintering conditions have been investigated in [11, 13, 16-19].

$BaTiO_3$, as additive in a varistor based ZnO, reduced the grain growth of ZnO as a function of the content of $BaTiO_3$. It is found that an excess of 9.6wt% $BaTiO_3$ leads to the $BaTiO_3$ phase segregation on the surface of the sample [2]. MgO-doped $BaTiO_3$ has been less studied. MgO is very often added at small amounts, less than 3mol.%. This MgO ratio is generally used in multi-component $BaTiO_3$-based ceramics, as high temperature capacitor in order to improve their temperature stability. MgO as an aliovalent in $BaTiO_3$ plays a decisive role in achieving ultra-broad temperature stability [20-23]. The effect of the aliovalent dopant on the bulk electrical conductivity is strongly dependent on its substitution site in the $BaTiO_3$ perovskite structure. Site replacement in the crystal lattice mainly depends on the dopant's ionic radius [8, 10, 13]. For small ions, with ionic radius r≤0.09nm, dopants preferentially occupy the Ti site. For intermediate ions, with 0.09nm<r<0.099nm, dopants can substitute either Ti or Ba depending on dopant concentration, sintering conditions and Ba/Ti molar ratio. For larger ions, with r≥0.099nm, dopants preferentially occupy the Ba sites. In [21-22], the solid solution between MgO (content <1.5%) and $BaTiO_3$ presents a XRD pattern, characteristic only of a single phase structure (BTO).This implies that Mg^{2+} ions have entered the unit cell maintaining the perovskite structure of solid solution. MgO phase in addition to the BTO phase, is detected for Mg contents, greater than 1.5% [21].

Electro-conductive composite ceramics are composed of an independent phase, of conglomerates and a continuous phase connecting mutually the independent phase of conglomerates. They are composed of an independent phase of conglomerates (50%-98% by weight) and of a continuous phase (2%-50% by weight) [24]. These ceramics can exhibit stable electro conductivity-temperature characteristics. They can be excellent in thermal shock resistance, in mechanical strength, and in chemical resistance. Concerning MgO-doped $BaTiO_3$ composite, only a few studies have been made [25]. In this paper, 5mol.%, 10mol.%, 15mol.%, 20mol.%, 30mol.%, and 50mol.% MgO-doped $BaTiO_3$ have been studied. The study aims to modify the BT-based materials characteristics such as T_c, electric permittivity and broaden the maxima peak. Sintering effect, microstructural evolution and incorporation degree of Mg into lattices ($BaTiO_3$) have been discussed as functions of the MgO content. Electric permittivity and resistance have been measured in temperatures ranging from 20°C to 400°C.

Corresponding author: Samira Boumous

II. EXPERIMENTAL PROCEDURE

High-purity commercial powder $BaTiO_3$ (code 01-081-2200), obtained from ALFA AESAR, was used as starting material with 70nm grain size. Using a conventional ceramic procedure, $BaTiO_3$ based varistor samples, doped with various contents of MgO (0, 5, 10, 15, 20, 30, 50mol.%.) were prepared. These samples are termed as BTM0, BTM5, BTM10, BTM15, BTM20, BTM30 and BTM50 respectively. Reagent grade oxides were mixed and homogenized in absolute ethanol media for 2 hours by planetary high-energy ball milling in a polyethylene bowl with zirconia balls. The slurry has been dried and sieved through a 200 mesh screen to produce granules without binder. The obtained powder was calcined at 1150°C for two hours in air at heating and cooling rates of 5°C/min. After drying and granulating with polyvinyl alcohol (PVA 4wt%) granules were uniaxially pressed into pellets under 20MPa and then CIPed at 200MPa. The pellets were placed in an alumina crucible and sintered at 1250°C for 2h in air at heating and cooling rates of 5°C/min, and silvered on both sides for electrical measurements. Silver electrodes were deposited by screen printing on each face. The sintered samples were all lapped and polished to be 1.0mm thick. The final samples had about 8mm i diameter and 1.0mm thickness. The samples were characterized by X-ray diffraction (XRD) using an automated diffractometer, Phillips PW-1710 type, coupled to a copper anode X-Ray tube. The microstructure of the samples was characterized by scanning electron microscopy (SEM type Hitachi-S2150) equipped with energy dispersive X-ray (EDX) spectrometer for elemental analysis. Dielectric measurements were carried out with the use of an impedance analyzer RLC (Wayne Kerr 6420). The measurements have been performed from room temperature up to 400°C, at a heating rate of 3°C/min. εr, tgδ and resistance were measured. Under an alternate electric field, the electric permittivity of the material can be expressed by a complex permittivity such $\varepsilon=\varepsilon'(\omega)-j\varepsilon''(\omega)$. The dielectric loss tangent is defined as $tg\delta=\varepsilon''/\varepsilon'$. In the following, we use the simplified notation ε_r and we will speak simply of permittivity to denote the real part of relative permittivity $\varepsilon'(\omega)$.

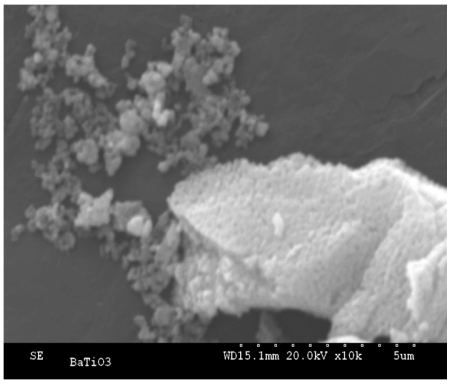

Fig. 1. SEM image of the commercial $BaTiO_3$ powder

III. RESULTS AND DISCUSSION

Commercial powder ($BaTiO_3$) was used. It is composed of a very small agglomeration, whereas the grains were very fine, of the order of 70nm. Figure 1 shows a SEM image of the commercial $BaTiO_3$ powder. We can see grain sizes smaller than one micrometer. In order to analyze the effect of MgO content on the microstructure and grain sizes, the samples have been characterized by SEM and XRD. Figure 2 shows the SEM images and EDX spectra of samples BTM0, BTM5 and BTM10 sintered at 1250°C. We can see in Figure 2(a) that the grain sizes of $BaTiO_3$, are larger in comparison with the ones of the same sample before sintering (Figure 1). They are larger than 1μm, while some are even larger than 10μm. The bimodal microstructure of fine and large matrix grains can be attributed to the temperature effect, as in the case of ZnO [2] and to presence of titanium oxide. The EDX spectrum characteristic of BTM0 (Figure 3(a)) indicates that, there are 60.30atom% of oxygen, 20.77atom% of Ti and 18.84atom% of Ba.

(a)

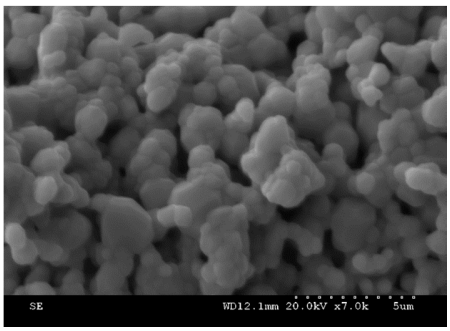

(b)

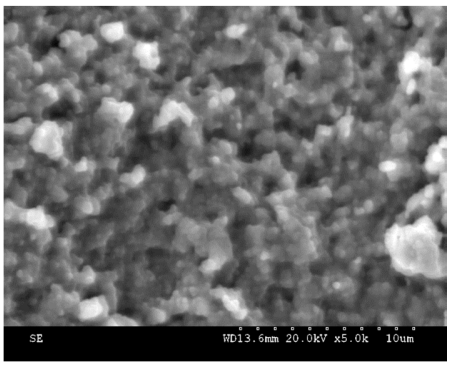

(c)

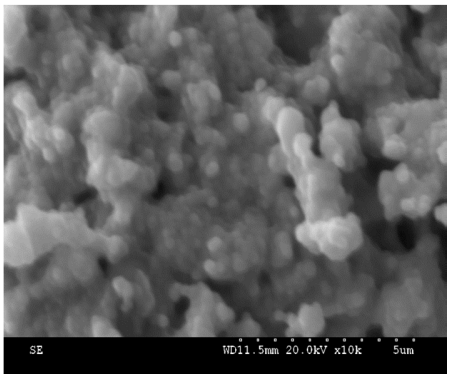

Fig. 2. SEM image of MgO-doped $BaTiO_3$ after sintering at 1250°C (a) BTM0, (b) BTM5, (c) BTM10

The grain size of BTM0 (pure) has increased under the temperature effect. Figures 2(b) and 3(b) show the morphology

and EDX spectrum of the sample BTM5. We can see that the grains are smaller. The surface morphology revealed some clear grain shapes. Figure 2(b) is brighter than Figure 2(a). We can see some bright domains, characteristics of MgO. The incorporation of MgO particles into the matrix is confirmed by EDX spectrum (Figure 3(b)). Au peak artifacts of sample preparation and support grid are noticed. In Figure 2(c), of the sample BTM10, the brightness domains are greater, the grain sizes are smaller and the brightness is stronger than that of Figure 2(b), since MgO content is greater than that of the samples BTM0 and BTM5.

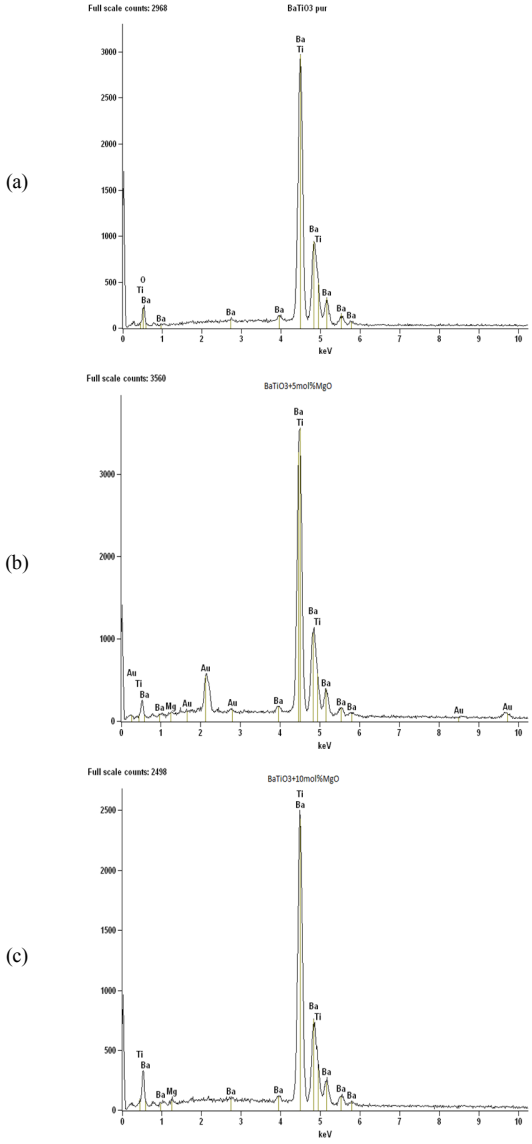

Fig. 3. EDX spectrum of MgO-$BaTiO_3$ compared with pure $BaTiO_3$. (a) BTM0, (b) BTM5, (c) BTM10

We can see the effect of MgO on the microstructure of the sample. The doping with MgO led to a consequent decrease in the grain size. The samples sintered at 1250°C show that grain sizes are smaller, whereas, undoped $BaTiO_3$ exhibits larger grain sizes (greater than 1μm). The most large grain size was estimated to be 10μm. For the sample BTM10, the grain size was in the order of 300nm. The result is in agreement with the findings in [21]. Incorporation of MgO particles in $BaTiO_3$ led to the grain growth inhibition of the composite. Even in other system such as $(Ba_{1-x}Ca_x)_mTiO_3$–MgO–SiO_2, MgO has been detected in the grain boundary region where MgO acts as a grain growth inhibitor [8, 26]. It is thus confirmed that in a MgO–$BaTiO_3$ system the grain growth is inhibited by the secondary phase which can be due to excess of MgO, existing in the grain boundary.

EDX mapping of elemental distribution of Ba, Ti, Mg and O has shown that MgO is highly dispersed in the $BaTiO_3$ matrix. We can see that the density of Mg in the BTM10 sample is greater than that of the sample BTM5. The distribution of the chemical elements is homogenous except for Mg in BTM10 probably near the grain boundaries where the solid solutions can be located. The non-homogeneity is characterized by a strong concentration in these regions. These are the dark regions in the SEM image representing the morphology of the sample. The SEM image and mapping of elemental distribution shows that $BaTiO_3$ seems to be covered with MgO particles.

A. X-Ray Diffraction

The diffraction pattern of X-ray (XRD) of these powders was performed for 45min at angle of 2θ, in temperatures ranging from 20°C to 80°C. The XRD spectra of the samples, BTM0, BTM5 and BTM10 sintered at 1250°C, are shown in Figure 4. The pure $BaTiO_3$ spectrum has been used as a reference.

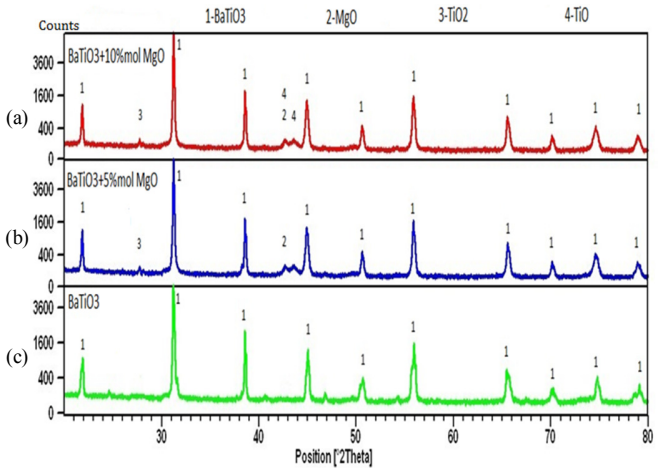

Fig. 4. XRD spectra of (a) BTM10, (b) BTM5 and (c) BTM0 sintered at 1250°C

1) BTM0

A representative XRD spectrum of the sample BTM0 is shown in Figure 4(c). The XRD study confirms the formation of the cubic system. All diffraction peaks coincide to that one of reference code 01-074-1964 where lattice parameter was equal to 4.0060Å. The obtained diffraction pattern is characteristic of a single perovskite phase.

2) BTM5

The XRD spectrum of the sample BTM5 (Figure 4(b)), reveals that the microstructure consists of three phases: $BaTiO_3$ grain (primary phase) characterized by a peak appearing at an angle of 2θ=31.559° and corresponding to (110) reflection plane. The other phases, MgO and TiO_2 are characterized by peaks appearing, at angles 2θ=42.917° and 2θ=28.527° and correspond to (200) and (421) refection planes respectively. The peak corresponding to the reflection plane is smaller (421). The parameters of these phases are given in the Table I. The increase in lattice constant of MgO-doped $BaTiO_3$, supports that Mg^2+ ions occupy Ti sites and expand the cell size, which is compatible with the acceptor doped behavior of MgO-doped $BaTiO_3$. Three phases are detected in BTM5. The result suggests that the solubility limit of MgO in $BaTiO_3$ has been exceeded whereas authors in [21] evaluate it between 1 and 1.5 at.%. They found only a second phase (MgO) from 2 at.% of MgO. In [22] where MgO content was only 1.0 vol%, the secondary phase (MgO) has not been detected. However, our samples contain more than 5 mol% MgO. The solid solution between MgO and BTO occurred by dissolution of a low amount of MgO (<1.5 at.% MgO) into $BaTiO_3$ and Mg^{2+} replaces Ti^{4+}, since the ionic radius of Mg^{2+} is larger than that of Ti^{4+}. This result is in agreement with [8, 16, 21, 22]. As our samples contain more than 1.5 at.% MgO, other phases of MgO and TiO_2 have been detected. MgO phase is the non-dissolved excess which is located in the grain boundaries. Furthermore, TiO_2 phase was formed via the reaction of MgO with $BaTiO_3$. The Ti atoms seem also segregated in the grain boundaries under oxide form. The segregation phenomenon is explained below using the energies of oxides formation. Otherwise, in the multi-component $BaTiO_3$-based ceramics, the Ti-rich phase forms via the reaction of excess TiO_2 with $BaTiO_3$ but MgO addition suppresses the Ti-rich phase as reported in [20]. Our bi-component sample (BTM5) seems to be insufficient to suppress the Ti-rich phase.

TABLE I. PARAMETERS OF CHARACTERISTIC PHASES – BTM5

Phase	Reference code	Crystal system	a (Å):	b (Å):	c (Å):	Density [g/cm^3]
$BaTiO_3$	01-075-0461	Cubic	4.0119	4.0119	4.0119	6.00
MgO	01-078-0430	Cubic	4.2112	4.2112	4.2112	3.56
TiO_2	01-088-1175	Tetragonal	4.5172	4.5172	2.9400	4.42

3) BTM10

The XRD spectrum of the sample BTM10 (Figure 4(a)) reveals that the microstructure consisted mainly of four phases: i) A primary phase ($BaTiO_3$ grains) characterized by a peak appearing at an angle 2θ=31.559° and corresponds to (110) reflection plane, ii) the MgO phase characterized by a peak appearing at an angle 2θ=42.906° and corresponds to (200) reflection plane, iii) the TiO_2 phase characterized by a peak appearing at an angle 2θ=27.911° and corresponding to (110) reflection plane, and finally iv) the TiO phase characterized by a peak appearing at an angle 2θ=43.671° and corresponding to (240) reflection plane. The detection of TiO phase indicates that 10 mol.%, as ratio of MgO, begins to reduce a part of TiO_2 phase into TiO phase. The parameters of these phases are given in Table II. We can see that MgO density has increased in comparison with the density of BTM5 (Table I), while those of $BaTiO_3$ and TiO_2 have kept the same values. The result is in agreement with [27], and indicates that the amount of intergranular pores is decreasing with increasing MgO. Consequently, the hardness of the $BaTiO_3$-MgO composite increased with increase in the MgO content.

TABLE II. PARAMETERS OF CHARACTERISTIC PHASES – BTM10

Phase	Reference code	Crystal system	a (Å):	b (Å):	c (Å):	Density [g/cm^3]
$BaTiO_3$	01-075-0461	Cubic	4.0119	4.0119	4.0119	6.00
MgO	01-078-0430	Cubic	4.2123	4.2123	4.2123	4.21
TiO_2	01-088-1175	Tetragonal	4.5170	4.5170	2.9400	4.42
TiO	01-072-0020	Monoclinic	5.8550	9.3400	4.1420	4.91

The models of diffusion and segregation, based on the sublimation enthalpies (bond energy) and the bond-breaking theory, are detailed in [28-30]. A preferential interaction coefficient (β) between the various atoms has been used to explain the evolution of the segregation. Concerning $BaTiO_3$, $\beta = \Delta G^0_{TiO2} - G^0_{BaO}$, $G^0_{TiO2,BaO}$ are the enthalpies of mixing of the intermetallic compound.

If β>0 there is interaction between Ba and oxygen. The segregation energy of Ba increases with the superficial concentration of O.

If β<0, the interaction between Ba and oxygen is of repulsive type. The element with the stronger tendency to segregate will push the other elements towards the bulk.

The obtained results concerning the sample BTM10 can be explained as follows.

Taking account of mixing enthalpies of components BaO (-609.4kJ/mol), MgO (-603.6kJ/mol), TiO_2 (-940kJ/mol), Mg^{2+} (-4.66.85kJ/mol), Ti (468kJ/mol), the component having the lowest heat, of sublimation, segregates to grain boundaries (or to the surface) and the element that has the stronger tendency to segregate, pushes the other elements towards the bulk. The calculation method of segregation energy is developed in [28-30] The TiO_2 enthalpy is the smaller (β=-331). This one segregates to grain boundaries and pushes MgO to the bulk, therefore Mg^{2+} substitutes for Ti^{4+}, since $Ti^{4+}$and Mg^{2+} ions have respectively, 0.605 and 0.720Å radius. Mg^{2+} ion is more likely to replace the Ti^{4+}ions instead of substituting for Ba^{2+} (1.61Å) [16]. Also, as the mixing enthalpies of components BaO and MgO are very close, the dissolution of MgO into $BaTiO_3$ was easier. Thus, when MgO content is greater than 1.5% (as carried out in [21]), the exceed is located in the grain boundaries or adsorbed at the surface [16, 23].

Concerning the fourth phase (TiO), it is known that beyond the oxygen solubility limit into titanium, different oxides can be formed such as Ti_6O, Ti_3O and TiO. However, stability of TiO has been obtained for an oxygen content between 34.5 at.% and 55.6 at.% [31]. The ratio of measured oxygen (60.25 at.%) is beyond this limit confirming the stability of the TiO phase. However, the driving force for the formation of the TiO_x originates from the respective energies of formation [32]. Segregation and Ti oxide formation depend on temperature, oxygen pressure and exposition time. TiO phase has been

detected only in BTM10 which contains 60.25 at.% oxygen. The energy of TiO formation is greater than that of TiO_2, therefore, it is expected to detect, especially TiO_2 but the result indicates reduction of TiO_2 into T_iO if one considers that the titanium segregates, under TiO_2 form. In this case, the chemical reaction of TiO_2 reduction can be considered. As the energy of TiO formation (-517.9kJ/mol) is greater than that of BaO, β will be greater than 0, since it is equal to 91.5 kJ/mol. Thus, TiO cannot segregate from grains towards grain boundaries. It is formed in the grain boundaries after the reduction of TiO_2 into TiO. The chemical reaction can be explained by using Ellingham diagram which shows the stability of the oxide as a function of temperature. A given metal can reduce the oxides of all metals whose lines lie above its own on the diagram. For Mg, $2Mg + O_2 \leftrightarrow 2MgO$ line lies below the $Ti + O_2 \leftrightarrow TiO_2$ line and so Mg can reduce TiO_2 into Ti. For higher content of MgO (greater than 5 mol%.) a part of TiO_2 is dissolved in the matrix, another part is reduced into TiO if the partial oxygen pressure in the matrix is lower than the equilibrium pressure value with the metal oxide at a given temperature. The remainder of TiO_2 is located in the grain boundaries. The result is in agreement with [20-22] since MgO was detected in the grain boundary regions of the system.

TiO_2 reduction into TiO, can be explained in the following way. Ti atoms, or a portion of them, can segregate in the grain boundaries under metallic form, instead of oxide form, and Mg atoms (under metallic form) diffuse into the matrix. Oxidations of Ti and Mg occur respectively in the grain boundaries and in the matrix. The formed oxides will depend of the oxygen amount in the matrix. If the oxygen amount located in the grains boundaries is low, TiO oxide can be formed, in addition to TiO_2 oxide. Finally, from the results of the microstructure, density data and XRD analysis as reported in [22] suggest that a quantity of MgO did not dissolve into the $BaTiO_3$ and remains present under the form of phase inclusion in the $BaTiO_3$ matrix and is located in the $BaTiO_3$ grain boundaries. Some Mg^{2+} ions have dissolved into the lattice to substitute Ti^{4+} ions on the B site of $BaTiO_3$ maintaining the perovskite structure of solid solution with additional phases such as TiO_2 and TiO when MgO content is greater than 5 mol%. The results confirm the ones carried out in [21]. Concerning the microstructure of this system, abnormal grain growth was found in pure $BaTiO_3$ with a 10μm average grain size. After addition of MgO particles into the system, the grain size decreased to less than 1μm for BTM5 and continuously decreased, with increasing MgO content (sample BTM10). MgO incorporation in the grain boundaries might be the grain growth inhibitor as reported in [8, 20-22].

High and stable electric permittivity, over a broad temperature range is significant for $BaTiO_3$-based ceramics due to their use in multi-layer ceramic capacitors [20, 23]. MgO is an important additive in $BaTiO_3$-based ceramics, because of its interesting electric properties. It has low electric permittivity (9 to 10.1), high dielectric strength (10 to 35kV/mm), apparent porosity null (%), tgδ around 9.10^{-3} and high use temperature (1800°C) [33-35]. The presence of MgO in $BaTiO_3$ matrix decreases the intergranular pores and increases the hardness of the MgO-$BaTiO_3$ composite [27]. The four samples (BMT15, BMT20, BMT30 and BMT50), have been processed to achieve ultra-broad-temperature stability.

B. Temperature Dependence of Dielectric Loss

Energy losses in ferroelectric materials are one of the most critical issues of high power devices. Ferroelectrics combined with MgO as a function of intrinsic and extrinsic defects should have other behavior regarding dielectric loss. The tgδ of a dielectric material is a useful indicator of dielectric loss. The samples with uniform microstructure, narrow grain size distribution, and less defects, exhibits low dielectric loss properties. Figure 5 shows the tgδ of the BTM0, BTM5, BTM10 samples over a temperature ranging from 25 to 300°C.

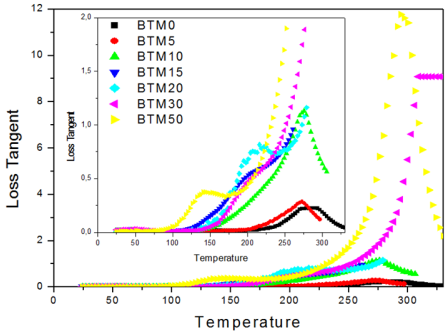

Fig. 5. tgδ versus temperature of all samples

BTM0 exhibits broad peak between 270°C and 290°C. The dielectric loss increases with increasing MgO content. The maximum values of tgδ for the three samples are ~ 0.15, 0.25 and 1.15 and correspond to temperatures 285°C, 270°C and 270°C respectively. For BTM5 and BTM10 the maximum is shifted to 270°C. The moving of loss peaks towards low temperature with increasing Mg content has been reported in [19]. In higher temperature range (200-500°C), the high dielectric loss peak may be induced by the polarization of free space charge associated with a thermally active relaxation process. The results are in agreement with [19-21, 36]. Authors in [21] attribute the result to the increase in the oxygen vacancies. In our case the oxygen vacancy concentration increases with increasing MgO content, since Mg^{2+} is an acceptor for $BaTiO_3$ and a double ionized oxygen vacancy (V_0^{++}) is formed in addition to the reduction of TiO_2 into TiO phase. However, MgO addition with multi-component $BaTiO_3$-based ceramics, for example $BaTiO_3$ co-doped with Y, Ga and Si [8], reduces dielectric loss, because of Y^{3+}doping. When the amount of MgO increases, (BTM15 and BTM20), the maxima of the loss curves shifted towards lower temperatures. These curves are characterized by oscillations around 200°C. At this temperature, the losses are greater than that of BTM5 and BTM10. The curve of the sample BTM20 presents a peak well resolved at 200°C. However, for the samples BTM30 and BTM50, the losses increase in comparison with that of BTM15 and BTM20, to reach respectively maxima at 9 and 12. These peaks are shifted towards higher temperatures (300°C) in comparison with that of BTM15 and BTM20. The increase of the losses can be so attributed to the increase of the oxygen

vacancies with the increase of MgO such as previously explained for BTM5 and BTM10.

C. Temperature Dependence of Electrical Resistance

Figure 6 shows the resistance versus temperature, in the temperature range from 25°C to 400°C, of all samples. It is a typical resistance-temperature characteristic of a $BaTiO_3$ based PTCR material. Impurities and lattice imperfections play an important role in the exhibition of the PTC effect, in the doped samples, since the losses are in connection with these imperfections [21]. Their conductivities are influenced by intrinsic defects such as oxygen vacancies and cation vacancies, and the extrinsic defects produced by dopant addition. Here, divalent Mg ions (under oxide form) are added to substitute Ti ions in the $BaTiO_3$. The conductivity seems to be influenced by oxygen vacancies generated by Ti, and the lattice deformation of the composite (4.0119Å) is larger than that of pure $BaTiO_3$ (4.0060) (see Tables II and III), proving that Mg substitutes Ti. TiO phase has been detected in BTM10, contributing to cation vacancy generation. The evolution of resistance versus temperature in Figure 6 shows the influence of these imperfections on the resistance. We can see that as the MgO content increases, the resistance is increasing along. However, the switching temperatures of the samples BTM0 and BTM5 are around 270°C, whereas that of BTM10 is located at 225°. The characteristic of BTM10 presents oscillations below the switching temperature (225°C). Authors in [17] attribute the temperature stability of the resistance, below the switching temperature (of PTCR ceramics), to the uniform grain size.

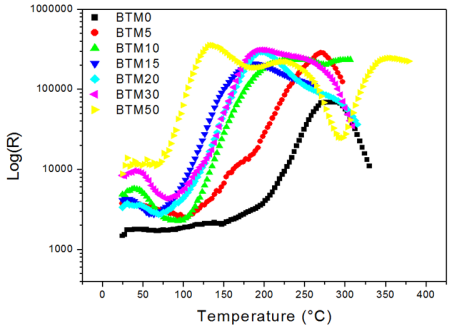

Fig. 6. Resistance versus temperature of all samples

Looking to the SEM image in Figure 2(a)-(b) corresponding to the samples BTM0 and BTM5, the grain sizes are lightly different, whereas the grain size, in the two samples, is in the order of μm. The switching temperature of the two samples is remains equal to 270°C. Only the amplitude of BTM5 is enhanced beyond $10^5\Omega$ because of MgO doping. However the grain size of BTM10 (Figure 2(c)) is smaller than that of the two precedent samples, in the order of a few hundred nanometers. We can see also that the resistance of this sample evolves differently. This one presents a broad peak where its maximum (smaller than that of BTM5) begins at 225°C and ends by oscillations until 350°C. The resistance, at room temperature, increases with MgO content increasing but, that of BTM10 decreases at 100°C, becomes smaller than that of BTM5, and afterwards increases again.

However, the curves of the samples BTM15, BTM20 are close in point of view form, and evolve in the same way with the sample BTM10. The maxima are less broad than that of BTM10 and their maxima are shifted towards 175°C. The minima are higher than the ones of the BM10. The sample BTM30 has a broad maximum which begins at 175°C and ends at 270°C. Its minimum is higher than the ones of BTM15 and BTM20. However, the curve of the sample BTM50 begins by a minimum, around 10000, greater than that of all other samples, and afterwards it increases to reach a maximum (around 30000), greater than that of all other samples. It is inferred that more MgO content reduces more TiO_2 into TiO or even into Ti, more cation vacancies are generated and the resistance is rising. This maximum appears at the Curie temperature (125°C) and ends with oscillations with a minimum well resolved at 300°C. These results confirm that, as MgO content increases, the dielectric loss of MgO-doped $BaTiO_3$ increases and Curie temperature shifts lower. Consequently, the resistance of the system increases. The result is in agreement with the findings in [21].

D. Electric Permittivity

Figure 7 shows the electric permittivity of MgO-doped $BaTiO_3$, for various MgO contents, in a temperature range from 20°C to 300°C. A sharp dielectric peak is recorded at Curie temperature (120°C) for BTM0. This T_C value has been found equal to the one reported in [20] for multicomponent $BaTiO_3$-based ceramics without MgO. Electric permittivity of BTMO reaches almost 6000 while in [20], it is only 1700. However, MgO effect on $BaTiO_3$ begins to appear on BTM5 by an enlargement of ε_r peak. ε_r maximum (5000) is located at 50°C. This enlargement of ε_r peak, has been indicated in [20] for samples containing 1.0wt%, 1.5wt% and 2wt% MgO, where maxima (around 2000) was located at 250°C. However, ε_r of BTM10 and BMT15, corresponding to the maximum and T_C=80°C, has been evaluated to 4500 and 4250 respectively. The minima are located around 240°C. A broaden peak has been recorded for BTM5. Mg plays a role, in Curie peak depression [8]. The ε_r peak is shifted towards lower temperatures. Authors in [21] attribute this result to the diffuseness of the phase transition. The electric permittivity decreases with increasing MgO content. This is in agreement with [8, 16, 21-23]. Our samples contain MgO, TiO_2 and TiO phases in the grain boundaries and even perhaps Ti in BTM30 and BTM50. BTM30 and BTM50 can be even two phase materials, with MgO as continuous phase. The grain boundary is a non-ferroelectric phase, therefore its electric permittivity is lower. Otherwise, the permittivity at room temperature can be explained by the ionic polarization. This one can be calculated using the Clausisus-Mossotti equation [8]. ε_r decreases with increasing Mg, because of the decrease in ionic polarizability (α) of the dipole as shown in [8]. The more the MgO content is, the smaller is the grain size, and the lower the ε_r. This justifies that ε_r changes as a function of MgO content over the studied temperature range (from ambient temperature to 250°C). At 250°C and beyond, the curves of ε_r (BTM0 and BTM10) present a minimum and increase again. However, for BTM5, the minimum appears at 350°C from which ε_r begins to increase slowly but remains smaller than that of BTM0 and BTM10. Concerning the samples BTM20 and BTM 30, the

curve evolution of ε_r kept the same form but their maxima, evaluated respectively to 4250 and less than 4000, are shifted towards 100°C. With 20 mol.% of MgO and more (30 mol.%.) as dopant, T_C shifts slightly again towards higher temperatures. After the minimum located at 300°C, as we can see in Figure 7, the ε_r of BTM30 decreases in comparison with that of BTM20. This part of the curve is comparable with that of BTM10. The ε_r of BTM50 is equal to 500. It is 10 times smaller than that of BTM5 and 12 times smaller than that of BTM0. Its curve is characterized by small maxima at 120°C and 200°C and ends by an increase towards 1000 at 400°C. The ε_r of the sample BTM50 is close to the value found in [25] where $BaTiO_3$ and MgO were both in the ratios 50% in volume. The ε_r, of the two phase material depends not only on the electric permittivity of the two phases (MgO and $BTiO_3$), but it is highly affected by the structure (phase distribution and grain size) and the stress level between the phases as a result of the differences in their thermal expansion result [25]. The two phases, are promising for the development of high electric permittivity and high dielectric strength capacitors, therefore, the breakdown voltage is expected to be high, since the paraelectric (MgO) phase is continuous at this concentration [25]. Our results confirm the findings in [25] since TiO_2 and TiO phases have vanished in BTM50. Sample BTM50 is a two phase material which is promising to have excellent thermal shock resistance, mechanical strength, and chemical resistance preperties.

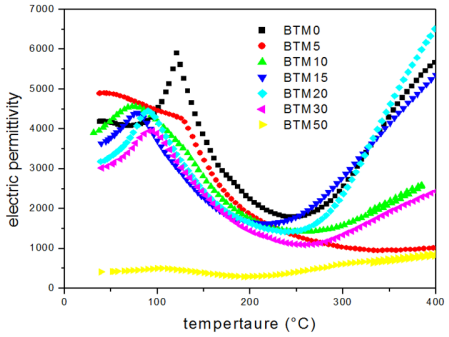

Fig. 7. Temperature dependence of electric permittivity

IV. CONCLUSION

The effects of MgO additions on the microstructure and the dielectric properties of $BaTiO_3$, have been studied. Oxides MgO and TiO_2 have been detected in the sample BTM5. MgO, TiO_2 and TiO were detected in the sample BTM10. MgO addition at 10 mol.%. and more, reduces the TiO_2 phase into TiO phase and can be even reduced into Ti phase. The grain size strongly depends on the MgO content. The average grain size of pure $BaTiO_3$ was near 10µm, whereas that of doped samples was about 1µm for BTM5 and some hundred nanometers for BTM10. The bimodal microstructure of fine and large matrix grains in BTM0 has been attributed to the temperature effect and to the presence of titanium oxide. ε_r decreases with increasing MgO content, while grain size and ε_r decrease. The electric permittivity of BTM50 was 12 times smaller than that of BTM0.The maximum peak was broader for increased MgO content. The T_C of BTM10 and BTM15 has been evaluated to 80°C, and to 100°C for BTM20 and BTM30. Beyond 15mol.% MgO, T_C is shifted again towards higher temperatures. The Curie temperature of BTM50 was equal to that of BTM0 (120°C). The conductivity is influenced by intrinsic defects, oxygen vacancies, and cation vacancies. The extrinsic defects were produced by dopant addition. Divalent ions (Mg) substitute Ti ions. Consequently, the conductivity was influenced by oxygen vacancies generated by Ti and the lattice deformation of the composite. The dielectric loss increases strongly with increasing MgO content. The loss peak, shifts towards low temperatures with increasing MgO content, whereas it may be induced by the polarization of free space charge associated with a thermally active relaxation process. The highest loss ($tg\delta$=12) has been measured on the BTM50, whereas that of BTM30 was equal to 9. The lowest loss has been measured on BTM0 ($tg\delta$=0.2) and BTM5 ($tg\delta$=0.3). TiO_2 and TiO phases have probably vanished in BTM30 and BTM50 samples. These samples, particularly BTM50, can be considered as two-phase materials, which is promising regarding shock resistance, mechanical strength and chemical resistance properties.

REFERENCES

[1] H. R. Rukmini, R. N. P. Choudary, V. V. Rao, "Structural and dielectric properties of $Pb_{0.91}(La,K)_{0.09}(Zr_{0.65}Ti_{0.35})_{0.9775}O_3$ ceramics", Journal of Materials Science, Vol. 34, No. 19, pp. 4815-4819, 1999

[2] F. Kharchouche, S. Belkhiat, D. E. C. Belkhiat, "Non-linear coefficient of $BaTiO_3$-doped ZnO varistor", IET Science, Measurement & Technology, Vol. 7, No. 6, pp. 326-333, 2013

[3] L. Madani, S. Belkhiat, A. Berrag, S. Nemdili, "Investigation of dielectric behavior of water and thermally aged of XLPE/$BaTiO_3$ composites in the low-frequency range", International Journal of Modern Physics B, Vol. 29, No. 27, pp. 1550186-155191, 2015

[4] M. N. Vijatovic, J. D. Bobic, B. D. Stojanovic, "History and Challenges of Barium Titanate: Part I", Science of Sintering, Vol. 40, No. 2, pp. 155-165, 2008

[5] D. Y. Lu, X. Y. Sun, B. Liu, J. L. Zhang, T. Ogata, "Structural and dielectric properties, electron paramagnetic resonance, and defect chemistry of Pr-doped $BaTiO_3$ ceramics", Journal of Alloys and Compounds, Vol. 615, pp. 25-34, 2014

[6] X. Huang, H. Liu, H. Hao, S. Zhang, Y. Sun, W. Zhang, L. Zhang, M. Cao, "Microstructure effect on dielectric Properties of MgO-doped $BaTiO_3$–$BiYO_3$ ceramics", Ceramics International, Vol. 41, No. 6, pp. 7489-7495, 2015

[7] S. D. Chavan, S. G. Chavan, D. J. Salunkhe, "Dielectric and Ferroelectric Properties of $(Ba_{0.95}Ca_{0.05})$ $(Ti_{0.90}Zr_{0.1})O_3$ Composition", Internal Journal of Multidisciplinary Research and Development, Vol. 1, No. 7, pp. 114-116, 2014

[8] M. J. Wang, H. Yang, Q. L. Zhang, Z. S. Lin, Z. S. Zhang, D. Yun, L. Hu, "Microstructure and dielectric properties of $BaTiO_3$ ceramic doped with yttrium, magnesium, gallium and silicon for AC capacitor application", Materials Research Bulletin, Vol. 60, pp. 485-491, 2014

[9] M. Aghayan, A. Khorsand Zak, M. Behdani, A. Manaf Hashim, "Sol–gel combustion synthesis of Zr-doped $BaTiO_3$ nanopowders and ceramics: Dielectric and ferroelectric studies", Ceramics International Vol. 40, pp. 16141-16144, 2014

[10] D. Ma, X. Chen, G. Huang, J. Chen, H. Zhou, L. Fang, "Temperature stability, structural evolution and dielectric properties of $BaTiO_3$–$Bi(Mg_{2/3}Ta_{1/3})O_3$ perovskite ceramics", Ceramics International, Vol. 41, No. 5, pp. 7157-7161, 2015

[11] J. J. Zhao, Y. P. Pu, P. P. Zhang, L. Cheng, S. J. Li, L. Feng, "Effect of $Na_2Ti_6O_{13}$ addition on the microstructure and PTCR characteristics of $Ba_{0.94}(Bi_{0.5}K_{0.5})_{0.06}TiO_3$ ceramics", Ceramics International Vol. 41, No. 3, pp. 4735-4741, 2015

[12] M. B. Smith, K. Page, T. Siegrist, P. L. Redmond, E. C. Walter, R. Seshadri, L. E. Brus, M. L. Steigerwald, "Crystal Structure and the

Paraelectric-to-Ferroelectric Phase Transition of Nanoscale $BaTiO_3$", Journal of the American Chemical Society, Vol. 130, pp. 6955-6963, 2008

[13] Y. L. Chen, S. F. Yang, "PTCR effect in donor doped barium titanate: review of compositions, microstructures, processing and properties", Advances in Applied Ceramics, Vol. 110, No. 5, pp. 257-269, 2011

[14] S. Urek, M. Drofenik, "PTCR behaviour of highly donor doped $BaTiO_3$", Journal of the European Ceramic Society, Vol. 19, No. 6, pp. 913-916, 1999

[15] J. Daniels, K. H. Hardtl, R. Wernicke, "PTC effect of barium titanate", Philips Technical Review, Vol. 38, No. 3, pp. 73-82, 1979

[16] S. Park, M. H. Yang, Y. H. Han, "Effects of MgO coating on the sintering behavior and dielectric properties of $BaTiO_3$", Materials Chemistry and Physics, Vol. 104, No. 2, 261-266, 2007

[17] M. Ma, Y. Wan, Y. Lu, W. Wu, Y. Li, "Effect of ball mill method on microstructure and electrical properties of $BaTiO_3$ based PTCR ceramics", Ceramics International, Vol. 41, pp. S804-S808, 2015

[18] G. D. Silveira, M. F. S. Alves, L. F. Cotica, R. A. M. Gota, W. J. Nascimento, D. Garcia, J. A. Eiras, L. A. Santos, "Dielectric investigations in nanostructured tetragonal BaTiO3 ceramics", Materials Research Bulletin, Vol. 48, No. 5, pp. 1772-1777, 2013

[19] J. Miao, Z. Zhang Z. Liu, Y. Li, "Investigation on the dielectric properties of Mg-doped $(Ba_{0.95}Ca_{0.05})(Ti_{0.85}Zr_{0.15})O_3$ ceramics", Ceramics International, Vol. 41, S487-S491, 2015

[20] L. Li, M. Wang, Y. Liu, J. Chen, N. Zhang, "Decisive role of MgO addition in the ultra-broad temperature stability of multicomponent $BaTiO_3$-based ceramics", Ceramics International, Vol. 40, No. 1, pp. 1105-1110, 2014

[21] W. Cai, C. L. Fu, J. C. Gao, C. X. Zhao, "Dielectric properties and microstructure of Mg doped barium titanate ceramics", Advances in Applied Ceramics, Vol. 110, No. 3, pp. 181-185, 2011

[22] C. Vittayakorn, D. Bunjong, R. Muanghlua, N. Vittayakorn, "Characterization and properties of $BaTiO_3$/MgO nanocomposite ceramics", Journal of Ceramic Processing Research, Vol. 12, No. 5, pp. 493-495, 2011

[23] J. S. Park, Y. H. Han, "Effects of MgO coating on microstructure and dielectric properties of $BaTiO_3$", Journal of the European Ceramic Society, Vol. 27, No. 2, pp. 1077-1082, 2007

[24] H. Yamamoto, S. Sendai, H. Ninomiya, Electroconductive Composite Ceramics, US Patent US4110260 A, 1978

[25] J. A. Zaykoski, C. A. Martin, I. G. Talmy, G. Zoski, "Two-Phase Ceramic Dielectrics", in: Advances in Dielectric Materials and Electronic Devices: Proceedings of the 107th Annual Meeting of The American Ceramic Society, Baltimore, Maryland, USA 2005, Vol. 174, John Wiley & Sons, 2012

[26] A. Al-Shahrani, S. Abboudy, "Positive temperature coefficient in Ho-doped $BaTiO_3$ ceramics", Journal of Physics and Chemistry of Solids, Vol. 61, No. 6, pp. 955-959, 2000

[27] S. Rattanachan, Y. Miyashita, Y. Mutoh, "Fracture Toughness of $BaTiO_3$-MgO Composites Sintered by Spark Plasma Sintering", 8th International Symposium on Fracture Mechanics of Ceramics, Houston, USA, February 25-28, 2003

[28] S. Belkhiat, F. Keraghel, "Oxygen and Carbon Effect on the Segregation Energy of Be on Cu-4at.%-Be Alloy Surface", International Review of Physics, Vol. 1, pp. 258, 2007

[29] S. Belkhiat, F. Keraghel, "Characterisation of Al-3.49wt%-Li Alloy Oxidised Surface Using Auger Electron Spectroscopy", Romanian Journal of Physics, Vol. 52, No. 3-4, pp. 309-317, 2007

[30] S. Belkhiat, F. Keraghel, "Hydrogen and Carbon Effect on Cu-4% at. Be Alloy Oxidised Surface", available at: https://arxiv.org/ftp/arxiv/papers/1011/1011.3875.pdf

[31] P. Simon, Synthese des Danoparticules d'Oxyde de Titanate par Pyrolyse Laser. Etude des Proprietes Optiques de la Structure Electronique, PhD Thesis, Universite Paris Sud XI, 2011 (in French)

[32] S. Le Moal, M. Moors, J. M. Essen, C. Breinlich, C. Becker, K. Wandelt, "Structural and compositional characterization of ultrathin titanium oxide films grown on Pt_3Ti (111)", Journal of Physics: Condensed Matter, Vol. 25, No. 4, pp. 45013, 2013

[33] B. D. Evans, M. Stapelbrock, "Fusion/fission neutron damage ratio for alumina", Journal of Nuclear Materials, Vol. 85-86, pp. 497-502, 1979

[34] Y. Y. Chen, M. M. Abraham, M. T. Robinson, J. B. Mitchell, R. A. Van Konynenburg, "Production of point defects in 14.8 MeV neutron - irradiated MgO", International Conference on Radiation Effects and Tritium Technology Fusion Reactors, Gatlinburg, USA, 1975

[35] J. Mazierska, D. Ledenyov, M. V. Jacob, J. Krupka, "Precise microwave characterization of MgO substrates for HTS circuits with superconducting post dielectric resonator", Superconductor Science and Technology, Vol. 18, No. 1, pp. 18-23, 2005

[36] G. Liu, S. Zhang, W. Jiang, W. Cao, "Losses in Ferroelectric Materials", Materials Science and Engineering: R: Reports, Vol. 89, pp. 1-48, 2015